Quantitative proteomics revealed a tight correlation between mitotic phosphorylation/dephosphorylation and structural properties of substrate domains

Hiroya Yamazaki[1], Hidetaka Kosako[2], and Shige H. Yoshimura[1]*

[1]Graduate School of Biostudies, Kyoto University, Kyoto, Japan, [2]Division of Cell Signaling, Fujii Memorial Institute of Medical Sciences, Tokushima University, Tokushima, Japan.

*Corresponding author:
Shige H. Yoshimura
Laboratory of Plasma Membrane and Nuclear Signaling,
Graduate School of Biostudies, Kyoto University,
Yoshida Konoe, Sakyo-ku, Kyoto 606-8501, Japan
Tel & Fax: +81-75-753-7906
E-mail: yoshimura@lif.kyoto-u.ac.jp

Abstract

Protein phosphorylation plays inevitable roles in the regulation and the progression of mitosis. More than ten thousands of phosphorylated residues and their responsible kinases have so far been identified by a number of proteomic analyses. While some of those phosphosites have been demonstrated to affect either protein-protein interaction or catalytic activity of the substrate protein, the effect of most mitotic phosphosites remain unclarified. In this study, we tried to extract structural properties of mitotic phosphosites and neighboring residues, and find a role of heavy phosphorylation at non-structured domain. A quantitative mass spectrometry of mitosis-arrested and non-arrested HeLa cells identified more than 4,100 and 1,900 residues which are significantly phosphorylated, and dephosphorylated at mitotic entry, respectively. Calculating the disorder score of the neighboring amino acid sequence of individual phosphosites revealed that more than 70% of the phosphosites which are dephosphorylated existed in disordered regions, whereas 50% of phosphorylated sites existed in non-structured domain. There was a clear inversed co-relation between probability in non-structured domain and increment of phosphorylation in mitosis. These results indicate that at the entry of mitosis, a significant amount of phosphate group is removed from non-structured domains and attached to more structured domains. GO term analysis revealed that mitosis-related proteins are heavily phosphorylated, whereas RNA-related proteins are both dephosphorylated and phosphorylated, implying that heavy phosphorylation/dephosphorylation in non-structured domain of RNA-binding proteins may play a role in dynamic rearrangement of RNA-containing organelle, as well as other intracellular environments.

Introduction

Protein phosphorylation/dephosphorylation plays critical roles in a number of cellular events such as intracellular signaling, cell cycle regulation, and the progression of mitosis. A number of studies using mass spectrometry successfully identified tens of thousands of phosphorylation sites and drew an entire atlas of phosphorylated states, as well as their dynamic alterations in the cell cycle (1), during mitosis (2) (3) (4), and during cell differentiation and development (5, 6).

The effect of phosphorylation on the structure/function of a substrate protein has been elucidated by various structural biological approaches. An addition of a phosphate group to the hydroxyl group of the target residue (Ser, Thr, or Tyr) affects either i) an interaction with other proteins, ii) the access of a substrate to the catalytic center of the enzyme, or iii) local internal energy, which induces an allosteric effect on the other part(s) of the protein. In any cases, phosphorylation affects stereo-specific interaction between the substrate protein and other molecules, which ensures a tight regulation of biological reactions.

On the other hand, recent bioinformatics studies revealed that phosphorylation preferably occurs at intrinsically disordered regions (IDR) of proteins (7–9). Due to the lack of any secondary and tertiary structures, IDR had been supposed to serve as a flexible substrate not only for phosphorylation, but also for other post-translational modifications (8). Although structural and functional significance of the IDR phosphorylation has not been fully understood, there are some possible explanations. One possibility could be that an addition of phosphate group reduces the flexibility of the IDR, and enables a specific interaction. In a transcription factor Ets1, phosphorylation at a serine residue in IDR changes the structure of the IDR, and reduce the affinity for DNA (10). In regulatory light chain of smooth muscle myosin, phosphorylation at Ser19 in IDR induces the formation of an α-helix, which activates an actin-dependent ATPase activity (11–13).

Another possibility could be the reduction of stereo-specificity between kinase and substrate. Human genome encodes ~520 different kinases and ~150 phosphatases, which phosphorylate or dephosphorylate over 40,000 sites in more than 10,000 proteins (14, 15). It means that a single kinase (a phosphatase) can phosphorylate (dephosphorylate) many different substrate sequences. Indeed, bioinformatic and biochemical studies could identify only weak or no consensus sequences for individual kinases (16) and almost no consensus around the target residue of phosphatases. The existence of the target residue in IDR reduces the stereo-specificity of enzyme-substrate interaction, and enables multiple combinations between them.

Mitosis is one of the most drastic cellular events and is tightly regulated by phosphorylation. At the entry of mitosis, more than several thousands of residues have been known to be phosphorylated (1, 2). A number of kinases which function in mitosis, such as CDK1, Aurora kinase, Plk1, Bub1, and Haspin, etc., have been identified (reviewed in (17–21)). Dephosphorylation also plays essential roles both at the entry and the exit of mitosis (22, 23) (24, 25). More than 1,000 kinds of phosphosites are dephosphorylated during anaphase (26), and more than five hundreds are dephosphorylated at the entry of mitosis (2). For example, CDK1 is activated by dephosphorylation by Cdc25B/C (27, 28), and Cdc25C is partially activated by protein phosphatase

70 1 (27). These results indicate that a vast number of phosphate groups are transferred to and from the substrate
71 proteins during mitotic entry.
72 One of the unclarified problems on mitotic phosphorylation could be why and how a vast number of
73 phosphate groups are transferred from a set of proteins to a different set of proteins, and whether these different
74 sets of mitotic phosphosites are structurally different or not. Especially, the distribution of phosphosites in
75 structured or non-structured regions of the substrate proteins is an important cue to understand the structural
76 effect of phosphorylation/dephosphorylation. In this study, we performed phosphoproteomic analysis of cellular
77 proteins to quantify and compare individual phosphosites in mitosis and interphase, and analyzed the structural
78 properties (IDR or structured) of those sites. Analysis of more than 5,000 phosphosites revealed a clear
79 relationship between mitotic phosphorylation/dephosphorylation and IDR.
80
81 **Result**
82 **Quantitative proteomic analysis of phospho-proteins in mitosis**
83 Comparative proteomics was performed on phosphopeptides obtained from asynchronous and mitotic HeLa
84 cells. Tryptic peptides from two populations were labeled with tandem mass tag (TMT) reagents. LC-MS/MS
85 was performed after enrichment of phosphopeptides by TiO_2. Total 17,003 phosophopeptides were quantified
86 (Fig. 1A), and 15,368 of them were assigned to proteins in a database, which are distributed in 3,701 proteins.
87 For quantitative analysis of phophorylation, peptides with only a single phosphosite were extracted and assigned
88 with "mitotic abundance ratio", which indicates the enrichment of the phosphosite in mitosis over in interphase
89 ($\log_2$(M phase/Asynchronous)). When the phosphosite was detected in more than two different peptides, the
90 abundance ratio was averaged. As a result, 10,255 phosphorylation sites were quantified and were subjected to
91 further analyses, while 4,400 sites were found only in peptides carrying multiple phosphosites. Out of 10,255
92 sites, 9,656 had already been registered in the phosphoprotein database, PhophoSitePlus (29), indicating our
93 dataset contained ≈600 unreported phosphosites.
94 To extract phosphosites which are specifically up-regulated or down-regulated in mitosis, the p-value
95 of individual peptides was plotted against the mitotic abundance. Thresholding the p-value at 0.01 (Fig. 1A)
96 could extract two different populations of phosphosites, one in positive and the other in negative in mitotic
97 abundance (Fig. 1B). The positive group (UP group) contains 4,138 phosphosites which distributed in 1,955
98 proteins, and the negative group (DOWN group) contained 2,249 phosphosites in 1,372 proteins. There was a
99 significant number of proteins (686) which carry both UP and DOWN sites (Fig. 1C). A small peak found at
100 ≈2.4 (Fig. 1B) mainly corresponds to linker domains of C_2H_2 zinc finger proteins, which are known to be
101 phosphorylated in mitosis (30). The mitotic phosphosites, which had been known to be up-regulated, such as
102 S11 and S29 of histone H3.1 (31) and T161 of CDK1 (28), were found in UP group with the abundance ratio
103 of 2.4, 1.3 and 0.8 respectively. The phosphosites known to be down-regulated, such as T14 of CDK1 (28) was
104 found in DOWN group with the mitotic abundance of -0.7.

105 Gene ontology (GO) analysis was performed for UP and DOWN sites. We obtained the terms of
106 biological process from DAVID (32, 33), and evaluated the enrichment of GO terms in each group of proteins
107 (UP and DOWN sites) by dividing the number of proteins in each group by the total number of proteins in
108 individual GO terms (Fig. 1D). As expected, proteins related to mitotic chromosome were highly enriched in
109 UP sites. Interestingly, proteins related to RNA processing and splicing are highly enriched in both UP and
110 DOWN sites, implying that RNA-related proteins are regulated both by phosphorylation and dephosphrylation
111 in mitosis (see *Discussion*).
112 The larger number of UP sites than DOWN sites does not necessarily mean that the total amount of
113 phosphorylated proteins in a mitotic cell are larger than dephosphorylated ones. To examine this, the total
114 amount of phosphorylated proteins was quantitated by dot-blot analysis using pIMAGO (34) and compared
115 between interphase and mitosis. Careful quantification revealed that 5.4 fmol of phosphates were attached to
116 proteins in a single mitotic cell, whereas 3.8 fmol in an asynchronous cell. This corresponds to 4.7 and 3.3 mM
117 in a mitotic and an asynchronous cell, respectively (the volume of HeLa cell is supposed to be 1.16 pL (35)),
118 (Fig. S1A), indicating that the amount of phosphate group on proteins are 1.4 times higher in mitotic cells than
119 asynchronous cell. This is concomitant with a decrease of ATP concentration examined by a FRET probe (Fig.
120 S1B, C, E) (36, 37), which was inhibited by a universal kinase inhibitor, staurosporine (Fig. S2A, B). The
121 reduction of the ATP concentration was due neither to the cell swelling during mitosis (38, 39) (Fig. S1D), to
122 the rearrangement of actin cytoskeleton (Fig. S2C, D), nor the reduction of ATP supply (glycolysis and
123 oxidative phosphorylation) (Fig. S2E-H). These results indicate that both phosphorylation and
124 dephosphorylation occur during mitosis, but the amount of phosphorylation dominates over dephosphorylation.
125
126 **Mitotic dephosphorylation preferably occurs at non-structured regions**
127 The relationship between mitosis-specific phosphorylation/dephosphorylation and higher-order structure of the
128 polypeptides was then investigated. A previous study reported that phosphorylation tends to occur at non-
129 structured region (intrinsically disordered region, IDR) within the substrate protein (7). We evaluated
130 intrinsically disordered score of individual residues by IUPred method (40, 41). In this study, the minimum
131 length of the IDR was set as 30 (see *Materials and Methods*). Under this criterion, 23.4 % of Ser/Thr residues
132 in total cellular proteins exist in IDR (Fig. 2A). On the other hand, 59.6 % of 10,255 phosphosites quantified
133 by our proteomic analysis were assigned in IDR (Fig. 2A), demonstrating a strong tendency of phosphorylation
134 occurring in IDRs.
135 We then focus on the relationship between mitotic phosphorylation/dephosphorylation and IDR. As
136 shown in Figure 2A, 71.0 % of DOWN and 52.6 % of UP sites exist in IDR. Interestingly, a strong inverse
137 correlation between the abundance ratio and the probability in IDR was found; the IDR probability gradually
138 decreased from ~80 to 40% as the abundance ratio increases (Fig. B). These values are extremely high compared
139 to the average value of all Ser/The residues (23.4 %). These results demonstrate that phosphorylation generally

140 prefers to occur in IDR, and such preference is significantly strong in dephosphorylation at the entry of mitosis.
141 The amino acid residue of phosphosites were also tightly co-related to the mitotic abundance ratio.
142 As shown in figure 2C, more than 90 % of DOWN sites are serine, and threonine occupied only ~7.8 %. The
143 percentage of serine reduced as the mitotic abundance increased; 75.2% of UP sites were serine and 24.8 %
144 were threonine. This result indicated that mitotic dephosphorylation occurs mostly at serine residues, whereas
145 mitotic phosphorylation occurs both at serine and threonine. This might be partially related to the high
146 probability of IDR in DOWN sites as demonstrated in Fig. 2A, since serine has higher disorder probability than
147 threonine. Alternatively, this might be due to the preference of phosphatase. PP2A is known to have higher
148 preference for threonine than serine residues, and be inactivated at mitotic entry and re-activated in anaphase as
149 demonstrated previously (3, 23, 26, 42) (see *Discussion*).
150
151 **Non-conventional sequence motif specific to mitotic phosphorylation**
152 We then analyzed sequence motifs of UP and DOWN sites. The UP and DOWN phosphosites were assigned to
153 one of the following consensus sequences based on their flanking amino acids (from -6 to +6) ; "proline-directed"
154 ([pS/pT]-P), which is phosphorylated by CDK and MAPK, "acidophilic" ([pS/pT]-X-X-[D/E], [pS/pT]-X-
155 [D/E] or [D/E]-X-[pS/pT]), which is recognized by PLK1 and Casein kinase, "basophilic" ([K/R]-X-X-[pS/pT]
156 or [K/R]-X-[pS/pT]), which is phosphorylated by Aurora kinase, PKC, and PKA (2, 43), or "non-conventional",
157 which does not match to any of the three above.
158 As shown in Figure 3A, B, three conventional motifs ("proline-directed", "acidophilic" and
159 "basophilic") occupied more than 90 % (92.3 %) of DOWN sites, meaning that most of mitotic
160 dephosphorylation occur at one of the conventional motifs. Interestingly, the amount of phosphorylation at non-
161 conventional motifs was higher in UP sites than DOWN sites (Fig. 3A, Fig. S3), suggesting that there could be
162 a mitosis-specific non-conventional motif. The conventional and non-conventional motifs also showed a clear
163 contrast in the relationship between IDR probability and the mitotic abundance. As shown in Figure 3C, the
164 probability in IDR showed inverse correlations to the mitotic abundance ratio in all three conventional motifs,
165 as demonstrated in Figure 2A. In a clear contrast, the IDR probability of non-conventional motif increased as
166 the abundance ratio increased (Fig. 3C). The high IDR probability of UP sites is opposite to the conventional
167 motifs. These results suggest that non-conventional motifs in IDR are phosphorylated in mitosis.
168 We then analyzed the amino acid sequences of "non-conventional" motif. Logo analysis of 557 UP
169 phospho-serine and 79 UP phospho-threonine in non-conventional motifs found high frequency of basic
170 residues (K or R) at the carboxylic side (+2 - +6) of the phosphosite (Fig. 3D). Especially, K/R at +3 position
171 is distinct. On the other hand, clear consensus was not found at the amino-terminal side of the phosphosite,
172 except for a weak consensus of a hydrophobic residue at -2 position, and K/R at -6 position. This consensus is
173 distinct from any other known kinase motifs, including the conventional basophilic motif, which has basic
174 amino acids at -2 or -3 position. In a clear contrast, such consensus was not found in DOWN sites; 133 DOWN

175 phospho-serine and 20 DOWN phospho-threonine in non-conventional motifs showed no clear consensus (Fig.
176 3E). These results suggest that non-conventional basophilic motif is unique for mitotic specific phosphorylation
177 sites.

178 We conducted GO analysis for proteins carrying UP site in non-conventional motif (502 proteins).
179 In contrast to the GO term analysis for the entire phosphoproteins with UP site, proteins related to "mRNA
180 export from nucleus" are highly enriched in NCB motif (24 out of 502 proteins in non-conventional motif
181 (4.8%) vs. 50 out of 1,955 proteins in entire UP sites (2.6%)) (Fig. 3F). These proteins contain subunits of
182 nuclear pore complex (Nups), splicing factors, and other RNA binding proteins. Nups and proteins with
183 transcription regulator activity are known to carry a substantial amounts of IDRs (44, 45). These results, together
184 with dephosphorylation of RNA related proteins (Fig. 1D), imply that phosphorylation/dephosphorylation of
185 RNA-related proteins play important roles in the progression of mitosis.

186

187 **Discussion**

188 In this study, we conducted a comparative proteomic analysis of phosphorylated residues in mitosis and
189 interphase cells by using TMT-6plex labeling technique, which can provide the ratio of individual peptide
190 amount in six samples with high precision (46). This approach successfully extracted two different populations
191 of phosphopeptides which are up- or down-regulated at mitotic entry. Bioinformatic analyses of these
192 phosphopeptides revealed a clear correlation between the phosphorylation/dephosphorylation reactions and the
193 IDR probability of the substrate. The most striking outcome of our analysis is that although phosphorylation
194 generally tends to occur in IDR, it is more striking in mitotic dephosphorylation; more than 70 % of DOWN
195 sites exist in IDR, whereas only 50% of UP sites was found in IDR (Fig. 2A, B). This means that as a total, a
196 significant amount of phosphate groups are removed from IDR, and are introduced into more structured regions
197 upon the entry of mitosis. Although the significance of such apparent transition of phosphate groups from IDR
198 to structured regions has not been fully elucidated in this study, several intriguing cues had been obtained from
199 analyses of flanking amino acid sequences and gene ontology. i) Most of mitotic dephosphorylation occur at
200 serine residue (91.9 %), whereas phosphorylation occur at both serine and threonine (75.2%, 24.8 %) (Fig. 2C).
201 ii) proteins involved in mitotic chromosome segregation are heavily phosphorylated, whereas proteins related
202 to RNA splicing, metabolism are both dephosphorylated and phosphorylated (Fig. 1D), iii) a non-conventional
203 basic motif is preferably phosphorylated in mitosis (Fig. 3A, D, E). These results imply an intriguing correlation
204 between mitotic phosphorylation and dynamic higher-order assembly/disassembly of biomolecules (protein,
205 DNA and RNA). The followings are several discussions on the significance of such dynamic behavior of
206 biomolecules in the context of cellular functions.

207 One of the effects of phosphorylation on IDR could be transition of higher-order structures (10, 47,
208 48). Phosphorylation in IDR has been known to cause disorder-to-order or order-to-disorder transition. For
209 example, phosphorylation of 4E-BP2 induced the formation of four-stranded β-sheet and prevent the binding

210 of eIF4E (49). Phosphorylation of phospholamban at Ser16, on the other hand, induced a disruption of higher
211 order structure, which reduced the inhibitory effect of phospholamban on sarco(endo)plasmic Ca-ATPase
212 activity (50, 51).

213 Another possible effect of phosphorylation at IDR could be that it regulates phase transition of
214 biomolecules. Non-structured polypeptide of IDR has been demonstrated to play a key role for liquid-liquid
215 phase separation (52). It accommodates a number of promiscuous interactions to assemble a number molecules.
216 It was demonstrated that phase transition of protein liquid droplet was induced by
217 phosphorylation/dephosphorylation (53–55). For example, liquid-liquid phase separation of positively charged
218 artificial peptide and RNA complex is promoted by dephosphorylation of the peptide (56). A study using a short
219 hydrophobic peptide which forms hydrogel demonstrated that gel-sol transition could be reversibly induced by
220 phosphorylation-dephosphorylation cycle by kinase and phosphatase (57); the peptide hydrogel was
221 transformed into solution when kinase and ATP was added to the gel, and re-solidified when phosphatase was
222 added to the solution. Such phenomenon was also observed in a living cell. The assembly/disassembly of RNA
223 granules are regulated by phosphorylation/dephosphorylation of one of the subunits (58). Although the
224 mechanism is not fully understood, these lines of evidences imply a possible effect of
225 phosphorylation/dephosphorylation on a dynamic assembly/disassembly transition of biomolecules upon the
226 entry of mitosis. It might be the case that phosphate groups in IDRs weakly assemble the proteins in interphase,
227 and their removal (dephosphorylation) upon the entry of mitosis will induce drastic assembly of the proteins
228 into a stable complex. Alternatively, mitotic phosphorylation solubilizes/disassembles the protein complex, and
229 dephosphorylation in anaphase reassemble them. Indeed, phosphorylation of the proteins in splicing
230 speckle, pericentriolar-satellite and stress granule by DYRK3 disassembled these membraneless organelles in
231 mitosis (59). Such phosphorylation-dependent regulation of protein assembly/disassembly depends on the
232 flanking amino acid sequences of the substrate residue. Previous report demonstrated that the charge pattern,
233 rather than the net charge, was important for phase separation (60). An addition of a minus charge by
234 phosphorylation could enhance or disrupt the charge pattern and affect the progress of phase separation.

235 Our gene ontology analysis on UP and DOWN phosphosites revealed that RNA-related proteins are
236 preferably dephosphorylated and phosphorylated in mitosis (Fig. 1D). This result is intriguing in the context of
237 phosphorylation-dependent regulation of phase transition in intracellular compartments. Recent studies
238 demonstrated that structure and function of several intracellular compartments are maintained by phase
239 separation, in which RNA plays a role in the molecular assembly (61). P-granule is a cytoplasmic compartment
240 of germ line of C. elegans. P-granule is considered to be liquid-like condensate, which contains mRNA and
241 RNA-binding proteins and may function in posttranscriptional regulation (62, 63). Protein components of P
242 granule, such as PGL-3 and LAF-1, formed liquid droplet *in vtiro*, and mRNA affected the dynamics of these
243 proteins within a droplet (64) (65). Nucleolus is also considered as a compartment, in which proteins and RNAs
244 assembled via mechanism similar to phase separation (66). Nucleolar protein nucleophosmin formed a droplet

245 with rRNA *in vitro* (67). Phosphorylation at $Thr^{199, 219, 234, 237}$ by CDK1 reduced the affinity for rRNA (68), and
246 replacement of these Ser by Glu partially abolished nucleolar localization in HeLa cells (69), suggesting that
247 phosphorylation of nucleophosmin controls the dynamics of proteins and RNAs within a nucleolus. It might be
248 the case that the removal/addition of a large number of phosphate groups from/to IDRs of RNA-related proteins
249 induces dynamic rearrangements of nucleolus and other RNA-containing nuclear speckles upon the entry of
250 mitosis, which may disrupt these organelle and release a large amount of RNA molecules into the cellular plasm.
251 This will drastically change an intracellular environment, and may affect the assembly/disassembly dynamics
252 of other protein complexes, such as chromosome, which is known to contain preribosomal RNA and nucleolar
253 proteins on the surface (70, 71). It might be the case that chromosome condensation could be induced by
254 orchestrated effects of phosphorylation of chromosome-related proteins (Fig. 1D) and RNA-induced drastic
255 change of an intracellular environment. Further study will be required to elucidate this problem.

256 It was surprising that most of dephosphorylation at the entry of mitosis occurred at serine, and
257 phosphorylation at both serine and threonine (Fig. 2C), suggesting that threonine phosphorylation is a mitosis-
258 specific event. One of the possible interpretations of such threonine phosphorylation could be that it is coupled
259 with dephosphorylation at anaphase, and therefore involved in temporary phosphorylation of substrate protein
260 during early mitosis. There are several experimental evidences which support this. i) It was demonstrated that
261 dephosphorylation at anaphase and telophase preferably occur at threonine residue in HeLa cells (3, 26). ii) In
262 budding yeast, threonine residues are heavily phosphorylated at the entry of mitosis, and dephosphorylated in
263 anaphase by $PP2A^{Cdc55}$, which is ortholog of $PP2A^{B55}$ (23, 25, 42). iii) Biochemical analysis revealed that
264 $PP2A^{B55}$, one of the major phosphatases working in anaphase, preferably dephosphorylates threonine residues
265 than serine (72). iv) When our dataset of UP site was compared to dephosphorylation dataset previously reported
266 (26), 28.3% of threonine and 16.7% of serine residues were dephosphorylated in anaphase. These lines of
267 evidences suggest that threonine functions as a temporary substrate of phosphorylation, and regulates the
268 reaction which requires tightly-tuned temporal regulation during mitosis. A combination of kinase and
269 phosphatase enables such tight regulation. Although a structural background of threonine-specific reaction is
270 not so far clarified, it must be involved in the early-mitotic events such as chromosome condensation.

271 We found a mitosis-specific phosphorylation motif, which is similar to conventional basophilic motif
272 but different in the position of basic residues (Fig. 3D). Although it is distinct from any known phosphorylation
273 motifs, several candidates could be found in phosphoproteomic database (2). PKC has been known to function
274 in mitosis (73, 74), and phosphorylate a serine residue near basic amino acids. However, the consensus of
275 several PKC subtypes contain basic residues at C-terminal side as well (43). PKCε plays a role in resolving
276 mitotic DNA catenation (75). Our gene ontology analysis revealed that proteins related to sister chromatid
277 segregation were enriched in proteins carrying NBC motif. Another candidate might be AMPK, which is
278 activated when AMP level increases and ATP level decreases (76), and known to phosphorylates mitosis-related
279 proteins (77). Although primary consensus motif for AMPK is basophilic motif, a peptide carrying K/R at +3

280 position, which is same as NBC-motif, can also be phosphorylated *in vitro* (78). Out of 243 proteins so far
281 identified as a substrate of AMPK (77), 17.3% (42 proteins) were found as the proteins with UP sites in NBC-
282 motif in our study (Table S1). Furthermore, it is intriguing that the intracellular ATP level decreased during
283 early mitosis (Fig. S1B-D). These results imply the existence of ATP-dependent regulatory mechanism of
284 mitosis; decreased level of intracellular ATP by the activity of conventional kinases at the entry of mitosis may
285 activate AMPK, which then phosphorylates different sets of substrate proteins to proceed the mitotic process.
286 The activity of AMPK increased from early mitosis and began to decrease when starting cytokinesis (77), and
287 this is well match to the ATP level during mitosis (Fig. S1C).
288

289 **Material and Method**

290 **Cell culture and cell synchronization**

291 HeLa cells were cultured in dulbecco's modified eagle medium (DMEM) (SIGMA-aldrich) with 10 % FBS
292 (GIBCO) at 37℃ under 5% CO2. For mitosis arrested cells, we first treated cells with 2 mM thymidine
293 (SIGMA adrich) for 18 hrs. Then cells were washed with PBS (-) and released into DMEM with 10 % FBS for
294 1 hour. Following treatment with 0.2 μM nocodazole for 10 hours achieved 80% synchronization of HeLa cells
295 at mitosis.
296

297 **TMT labeling and mass spectrometry**

298 Asynchronous and mitosis-arrested HeLa cells in 100 mm cell culture dish (Corning) were washed twice with
299 5 mL of ice-cold Hepes-saline (20 mM Hepes-NaOH, pH7.5, 137 mM NaCl). 0.75 mL guanidine hydrochloride
300 buffer (6 M guanidine hydrochloride, 100 mM Tris-HCl (pH8.0), 2 mM DTT) was added, and cell lysates were
301 prepared in triplicate and frozen in liquid nitrogen. The lysates were dissolved by heating and sonication,
302 followed by the centrifugation at 20,000 x g for 15 min at 4°C. The supernatants were reduced in 5 mM DTT
303 at room temperature for 30 min and alkylated in 27.5 mM iodoacetamide at room temperature for 30 min in the
304 dark. Proteins were purified by methanol/chloroform precipitation and solubilized by 25 μL of 0.1% RapiGest
305 SF (Waters) in 50 mM triethylammonium bicarbonate. After repeated sonication and vortex, the proteins were
306 digested with 2 μg of trypsin/Lys-C mix (Promega) for 16 hr at 37°C. Peptide concentration was determined
307 using Pierce quantitative colorimetric peptide assay (Thermo Fisher Scientific). Approximately 150 μg of
308 peptides for each sample were labeled with 200 μg of TMT6-plex reagents (Thermo Fisher Scientific) for 1 hr
309 at room temperature. After the reaction was quenched with hydroxylamine, all the TMT-labeled samples were
310 pooled and acidified with trifluoroacetic acid (TFA). Phosphopeptides were enriched using 50 mg of
311 Titansphere Phos-TiO column (GL Sciences) in accordance with the manufacturer's instructions and then
312 fractionated using Pierce high pH reversed-phase peptide fractionation kit (Thermo Fisher Scientific). Eight
313 fractions were collected using 5%, 7.5%, 10%, 12.5%, 15%, 17.5%, 20%, and 50% acetonitrile (ACN). Each
314 fraction was evaporated in a SpeedVac concentrator and dissolved in 0.1% TFA.

315 LC-MS/MS analysis of the resultant peptides (1 μg each) was performed on an EASY-nLC 1200 UHPLC
316 connected to a Q Exactive Plus mass spectrometer through a nanoelectrospray ion source (Thermo Fisher
317 Scientific). The peptides were separated on a 75 μm inner diameter × 150 mm C18 reversed-phase column
318 (Nikkyo Technos) with a linear gradient from 4–20% ACN for min 0–180 and 20–32% ACN for min 180–220
319 followed by an increase to 80% ACN during min 220–230. The mass spectrometer was operated in a data-
320 dependent acquisition mode with a top 10 MS/MS method. MS1 spectra were measured with a resolution of
321 70,000, an automatic gain control (AGC) target of 3×10^6 and a mass range from 375 to 1,400 *m/z*. HCD MS/MS
322 spectra were acquired at a resolution of 35,000, an AGC target of 1×10^5, an isolation window of 0.4 *m/z*, a
323 maximum injection time of 100 msec and a normalized collision energy of 32. Dynamic exclusion was set to
324 30 sec. Raw data were directly analyzed against the Swiss-Prot database restricted to *Homo sapiens* using
325 Proteome Discoverer version 2.1 (Thermo Fisher Scientific) with Mascot search engine version 2.5 (Matrix
326 Science) for identification and TMT quantification. The search parameters were (a) trypsin as an enzyme with
327 up to two missed cleavages, (b) precursor mass tolerance of 10 ppm, (c) fragment mass tolerance of 0.02 Da,
328 (d) TMT of lysine and peptide N-terminus and carbamidomethylation of cysteine as fixed modifications, and
329 (e) phosphorylation of serine, threonine and tyrosine, acetylation of protein N-terminus and oxidation of
330 methionine as variable modifications. Peptides were filtered at a false-discovery rate (FDR) of 1 % using the
331 percolator node.
332
333 **Data analysis**
334 Data analysis was performed by Python2 or 3 and its library (Numpy, Scipy, Pandas, Matplotlib, Seaborn) using
335 Jupyter (IPython) Notebook. The latest version of phosphosites' dataset from PhosphoSitePlus (29) (Wed Nov
336 08 15:57:30 EST 2017) was used. For GO analysis, DAVID 6.8 (32, 33) was used. The term, "BP_5" was
337 obtained as biological process terms applying homo sapience as a back ground. The number of proteins of our
338 dataset in each term was divided by the total number of proteins in each GO term to evaluate the abundance of
339 the term. For IDR analysis, IUPred method (40, 41) was used. Position-specific estimations of energies of each
340 residue was calculated based on the method in Dosztányi's paper by Perl script. The residues with the energy
341 larger than -0.203 [aeu] were defined as intrinsically disordered residues according to IUPred method. Then the
342 stretch of amino acids with sequence of more than 30 intrinsically disordered residues were regarded as
343 intrinsically disordered region. LOGO analysis of the neighboring amino acids of phosphosites was performed
344 by using "PSP production" algorithm in PhosphoSitePlus (29).
345

346 1. Olsen J V, et al. (2010) Quantitative phosphoproteomics reveals widespread full phosphorylation site
347 occupancy during mitosis. *Sci Signal* 3(104):ra3.
348 2. Dephoure N, et al. (2008) A quantitative atlas of mitotic phosphorylation. *Pnas* 105(31):10762–10767.
349 3. Malik R, et al. (2009) Quantitative analysis of the human spindle phosphoproteome at distinct mitotic
350 stages. *J Proteome Res* 8(10):4553–4563.
351 4. Ohta S, Kimura M, Takagi S, Toramoto I, Ishihama Y (2016) Identification of Mitosis-Specific
352 Phosphorylation in Mitotic Chromosome-Associated Proteins. *J Proteome Res* 15(9):3331–3341.
353 5. Yue J, et al. (2017) Phosphorylation of Pkp1 by RIPK4 regulates epidermal differentiation and skin
354 tumorigenesis. *EMBO J* 36(13):1963–1980.
355 6. Roux MM, Radeke MJ, Goel M, Mushegian A, Foltz KR (2008) 2DE identification of proteins
356 exhibiting turnover and phosphorylation dynamics during sea urchin egg activation. *Dev Biol*
357 313(2):630–647.
358 7. Iakoucheva LM, et al. (2004) The importance of intrinsic disorder for protein phosphorylation. *Nucleic*
359 *Acids Res* 32(3):1037–1049.
360 8. Darling AL, Uversky VN (2018) Intrinsic disorder and posttranslational modifications: The darker side
361 of the biological dark matter. *Front Genet* 9(MAY):1–18.
362 9. Collins MO, Yu L, Campuzano I, Grant SGN, Choudhary JS (2008) Phosphoproteomic Analysis of the
363 Mouse Brain Cytosol Reveals a Predominance of Protein Phosphorylation in Regions of Intrinsic
364 Sequence Disorder. *Mol Cell Proteomics* 7(7):1331–1348.
365 10. Kasahara K, Shiina M, Higo J, Ogata K, Nakamura H (2018) Phosphorylation of an intrinsically
366 disordered region of Ets1 shifts a multi-modal interaction ensemble to an auto-inhibitory state. *Nucleic*
367 *Acids Res* 46(5):2243–2251.
368 11. Nelson WD, Blakely SE, Nesmelov YE, Thomas DD (2005) Site-directed spin labeling reveals a
369 conformational switch in the phosphorylation domain of smooth muscle myosin. *Proc Natl Acad Sci*
370 102(11):4000–4005.
371 12. Espinoza-Fonseca LM, Kast D, Thomas DD (2007) Molecular dynamics simulations reveal a disorder-
372 to-order transition on phosphorylation of smooth muscle myosin. *Biophys J* 93(6):2083–2090.
373 13. Espinoza-Fonseca LM, Kast D, Thomas DD (2008) Thermodynamic and structural basis of
374 phosphorylation-induced disorder-to-order transition in the regulatory light chain of smooth muscle
375 myosin. *J Am Chem Soc* 130(37):12208–12209.
376 14. Ardito F, Giuliani M, Perrone D, Troiano G, Muzio L Lo (2017) The crucial role of protein
377 phosphorylation in cell signalingand its use as targeted therapy (Review). *Int J Mol Med* 40(2):271–
378 280.
379 15. Horn H, et al. (2014) KinomeXplorer: An integrated platform for kinome biology studies. *Nat Methods*
380 11(6):603–604.

16. Rust HL, Thompson PR (2011) Kinase consensus sequences: A breeding ground for crosstalk. *ACS Chem Biol* 6(9):881–892.
17. Bazile F, St-Pierre J, D'Amours D (2010) Three-step model for condensin activation during mitotic chromosome condensation. *Cell Cycle* 9(16):3243–3255.
18. Wang G, Jiang Q, Zhang C (2014) The role of mitotic kinases in coupling the centrosome cycle with the assembly of the mitotic spindle. *J Cell Sci* 127(19):4111–4122.
19. Bayliss R, Fry A, Haq T, Yeoh S (2012) On the molecular mechanisms of mitotic kinase activation. *Open Biol* 2(11):120136–120136.
20. Nigg EA (2001) Mitotic kinases as regulators of cell division and its checkpoints. *Nat Rev Mol Cell Biol* 2(1):21–32.
21. Alvarez-Fernandez M, Malumbres M (2014) Preparing a cell for nuclear envelope breakdown: Spatio-temporal control of phosphorylation during mitotic entry. *BioEssays* 36(8):757–765.
22. Barr FA, Elliott PR, Gruneberg U (2011) Protein phosphatases and the regulation of mitosis. *J Cell Sci* 124(14):2323–2334.
23. Kim H, Fernandes G, Lee C (2016) Protein Phosphatases Involved in Regulating Mitosis: Facts and Hypotheses. *Mol Cells* 39(9):654–62.
24. Sullivan M, Morgan DO (2007) Finishing mitosis, one step at a time. *Nat Rev Mol Cell Biol* 8(11):894–903.
25. Wurzenberger C, Gerlich DW (2011) Phosphatases: Providing safe passage through mitotic exit. *Nat Rev Mol Cell Biol* 12(8):469–482.
26. Castro A, et al. (2015) Global Phosphoproteomic Mapping of Early Mitotic Exit in Human Cells Identifies Novel Substrate Dephosphorylation Motifs. *Mol Cell Proteomics* 14(8):2194–2212.
27. Perdiguero E, Nebreda AR (2004) Regulation of Cdc25C activity during the meiotic G2/M transition. *Cell Cycle* 3(6):733–737.
28. Timofeev O, Cizmecioglu O, Settele F, Kempf T, Hoffmann I (2010) Cdc25 phosphatases are required for timely assembly of CDK1-cyclin B at the G2/M transition. *J Biol Chem* 285(22):16978–16990.
29. Hornbeck P V., et al. (2015) PhosphoSitePlus, 2014: Mutations, PTMs and recalibrations. *Nucleic Acids Res* 43(D1):D512–D520.
30. Rizkallah R, Alexander KE, Hurt MM (2011) Global mitotic phosphorylation of C2H2 zinc finger protein linker peptides. *Cell Cycle* 10(19):3327–3336.
31. Crosio C, et al. (2002) Mitotic Phosphorylation of Histone H3 : Spatio-Temporal Regulation by Mammalian Aurora Kinases. 22(3):874–885.
32. Huang DW, Sherman BT, Lempicki RA (2009) Systematic and integrative analysis of large gene lists using DAVID bioinformatics resources. *Nat Protoc* 4(1):44–57.
33. Huang DW, Sherman BT, Lempicki RA (2009) Bioinformatics enrichment tools: Paths toward the

416 comprehensive functional analysis of large gene lists. *Nucleic Acids Res* 37(1):1–13.
417 34. Pan L, et al. (2015) Sensitive measurement of total protein phosphorylation level in complex protein
418 samples. *Analyst* 140:3390–3396.
419 35. Fujioka A, et al. (2006) Dynamics of the Ras/ERK MAPK cascade as monitored by fluorescent probes.
420 *J Biol Chem* 281(13):8917–8926.
421 36. Ahn E, Kumar P, Mukha D, Tzur A, Shlomi T (2017) Temporal fluxomics reveals oscillations in TCA
422 cycle flux throughout the mammalian cell cycle. *Mol Syst Biol* 13(11):953.
423 37. Maeshima K, et al. (2018) A Transient Rise in Free Mg 2+ Ions Released from ATP-Mg Hydrolysis
424 Contributes to Mitotic Chromosome Condensation. *Curr Biol*:1–8.
425 38. Son S, et al. (2015) Resonant microchannel volume and mass measurements show that suspended cells
426 swell during mitosis. *J Cell Biol* 211(4):757–763.
427 39. Zlotek-Zlotkiewicz E, Monnier S, Cappello G, Le Berre M, Piel M (2015) Optical volume and mass
428 measurements show that mammalian cells swell during mitosis. *J Cell Biol* 211(4):765–774.
429 40. Dosztányi Z, Csizmók V, Tompa P, Simon I (2005) The pairwise energy content estimated from amino
430 acid composition discriminates between folded and intrinsically unstructured proteins. *J Mol Biol*
431 347(4):827–839.
432 41. Dosztányi Z, Csizmok V, Tompa P, Simon I (2005) IUPred: Web server for the prediction of
433 intrinsically unstructured regions of proteins based on estimated energy content. *Bioinformatics*
434 21(16):3433–3434.
435 42. Godfrey M, et al. (2017) PP2ACdc55 Phosphatase Imposes Ordered Cell-Cycle Phosphorylation by
436 Opposing Threonine Phosphorylation. *Mol Cell* 65(3):393–402.e3.
437 43. Kreegipuu A, Blom N, Brunak S, Ja J (1998) Statistical analysis of protein kinase specifcity
438 determinants. *FEBS Lett* 430:45–50.
439 44. Patel SS, Denning DP, Fink AL, Uversky V, Rexach M (2003) Disorder in the nuclear pore complex:
440 The FG repeat regions of nucleoporins are natively unfolded. *Proc Natl Acad Sci* 100(5):2450–2455.
441 45. Haynes C, et al. (2006) Intrinsic disorder is a common feature of hub proteins from four eukaryotic
442 interactomes. *PLoS Comput Biol* 2(8):0890–0901.
443 46. Hogrebe A, et al. (2018) Benchmarking common quantification strategies for large-scale
444 phosphoproteomics. *Nat Commun* 9(1). doi:10.1038/s41467-018-03309-6.
445 47. Travers T, et al. (2015) Tandem phosphorylation within an intrinsically disordered region regulates
446 ACTN4 function. *Sci Signal* 8(378):1–10.
447 48. Fealey ME, Binder BP, Uversky VN, Hinderliter A, Thomas DD (2018) Structural Impact of
448 Phosphorylation and Dielectric Constant Variation on Synaptotagmin's IDR. *Biophys J* 114(3):550–
449 561.
450 49. Bah A, et al. (2015) Folding of an intrinsically disordered protein by phosphorylation as a regulatory

451 switch. *Nature* 519(7541):106–9.
452 50. Metcalfe EE, Traaseth NJ, Veglia G (2005) Serine 16 phosphorylation induces an order-to-disorder
453 transition in monomeric phospholamban. *Biochemistry* 44(11):4386–4396.
454 51. Chu G, Kranias EG (2003) Functional interplay between dual site phospholambam phosphorylation:
455 insights from genetically altered mouse models. *Basic Res Cardiol* 97(7):1–1.
456 52. Uversky VN (2017) Intrinsically disordered proteins in overcrowded milieu: Membrane-less
457 organelles, phase separation, and intrinsic disorder. *Curr Opin Struct Biol* 44:18–30.
458 53. Kwon I, et al. (2014) Phosphorylation-regulated binding of RNA polymerase ii to fibrous polymers of
459 low-complexity domains. *Cell* 156(1–2):374.
460 54. Guillén-Boixet J, Buzon V, Salvatella X, Méndez R (2016) CPEB4 is regulated during cell cycle by
461 ERK2/Cdk1-mediated phosphorylation and its assembly into liquid-like droplets. *Elife*
462 5(NOVEMBER2016):1–26.
463 55. Monahan Z, et al. (2017) Phosphorylation of the FUS low-complexity domain disrupts phase
464 separation, aggregation, and toxicity. *EMBO J* 36(20):e201696394.
465 56. Aumiller WM, Keating CD (2016) Phosphorylation-mediated RNA/peptide complex coacervation as a
466 model for intracellular liquid organelles. *Nat Chem* 8(2):129–137.
467 57. Yang Z, Liang G, Wang L, Xu B (2006) Using a kinase/phosphatase switch to regulate a
468 supramolecular hydrogel and forming the supramolecular hydrogel in vivo. *J Am Chem Soc*
469 128(9):3038–3043.
470 58. Wang JT, et al. (2014) Regulation of RNA granule dynamics by phosphorylation of serine-rich,
471 intrinsically disordered proteins in C. elegans. *Elife* 3:1–23.
472 59. Rai AK, Chen JX, Selbach M, Pelkmans L (2018) Kinase-controlled phase transition of membraneless
473 organelles in mitosis. *Nature* 559(7713):211–216.
474 60. Nott TJ, et al. (2015) Phase Transition of a Disordered Nuage Protein Generates Environmentally
475 Responsive Membraneless Organelles. *Mol Cell* 57(5):936–947.
476 61. Lin Y, Protter DSW, Rosen MK, Parker R (2015) Formation and Maturation of Phase-Separated
477 Liquid Droplets by RNA-Binding Proteins. *Mol Cell* 60(2):208–219.
478 62. Updike D, Strome S (2010) P granule assembly and function in Caenorhabditis elegans germ cells. *J*
479 *Androl* 31(1):53–60.
480 63. Seydoux G (2018) The P Granules of C. elegans: A Genetic Model for the Study of RNA–Protein
481 Condensates. *J Mol Biol* 430(23):4702–4710.
482 64. Saha S, et al. (2016) Polar Positioning of Phase-Separated Liquid Compartments in Cells Regulated by
483 an mRNA Competition Mechanism. *Cell* 166(6):1572–1584.e16.
484 65. Elbaum-Garfinkle S, et al. (2015) The disordered P granule protein LAF-1 drives phase separation into
485 droplets with tunable viscosity and dynamics. *Proc Natl Acad Sci* 112(23):7189–7194.

486 66. Feric M, et al. (2016) Coexisting Liquid Phases Underlie Nucleolar Subcompartments. *Cell*
487 165(7):1686–1697.
488 67. Mitrea DM, et al. (2018) Self-interaction of NPM1 modulates multiple mechanisms of liquid-liquid
489 phase separation. *Nat Commun* 9(1):1–13.
490 68. Okuwaki M, Tsujimoto M, Nagata K (2002) The RNA Binding Activity of a Ribosome Biogenesis
491 Factor, Nucleophosmin/B23, Is Modulated by Phosphorylation with a Cell Cycle-dependent Kinase
492 and by Association with Its Subtype. *Mol Biol Cell* 13(June):2016–2030.
493 69. Negi SS, Olson MOJ (2006) Effects of interphase and mitotic phosphorylation on the mobility and
494 location of nucleolar protein B23. *J Cell Sci* 119(17):3676–3685.
495 70. Van Hooser AA, Yuh P, Heald R (2005) The perichromosomal layer. *Chromosoma* 114(6):377–388.
496 71. Hayashi Y, Kato K, Kimura K (2017) The hierarchical structure of the perichromosomal layer
497 comprises Ki67, ribosomal RNAs, and nucleolar proteins. *Biochem Biophys Res Commun*
498 493(2):1043–1049.
499 72. Pinna LA, Donella-Deana A (1994) Phosphorylated synthetic peptides as tools for studying protein
500 phosphatases. *BBA - Mol Cell Res* 1222(3):415–431.
501 73. Dai Z, Dulyaninova NG, Kumar S, Bresnick AR, Lawrence DS (2007) Visual Snapshots of
502 Intracellular Kinase Activity at the Onset of Mitosis. *Chem Biol* 14(11):1254–1260.
503 74. Martini S, et al. (2017) PKCε Controls Mitotic Progression by Regulating Centrosome Migration and
504 Mitotic Spindle Assembly. *Mol Cancer Res*:3–16.
505 75. Brownlow N, Pike T, Zicha D, Collinson L, Parker PJ (2014) Mitotic catenation is monitored and
506 resolved by a PKC-regulated pathway. *Nat Commun* 5(May):1–13.
507 76. Hardie DG (2007) AMP-activated/SNF1 protein kinases: Conserved guardians of cellular energy. *Nat*
508 *Rev Mol Cell Biol* 8(10):774–785.
509 77. Banko MR, et al. (2011) Chemical Genetic Screen for AMPKα2 Substrates Uncovers a Network of
510 Proteins Involved in Mitosis. *Mol Cell* 44(6):878–892.
511 78. Gwinn DM, et al. (2008) AMPK Phosphorylation of Raptor Mediates a Metabolic Checkpoint. *Mol*
512 *Cell* 30(2):214–226.
513

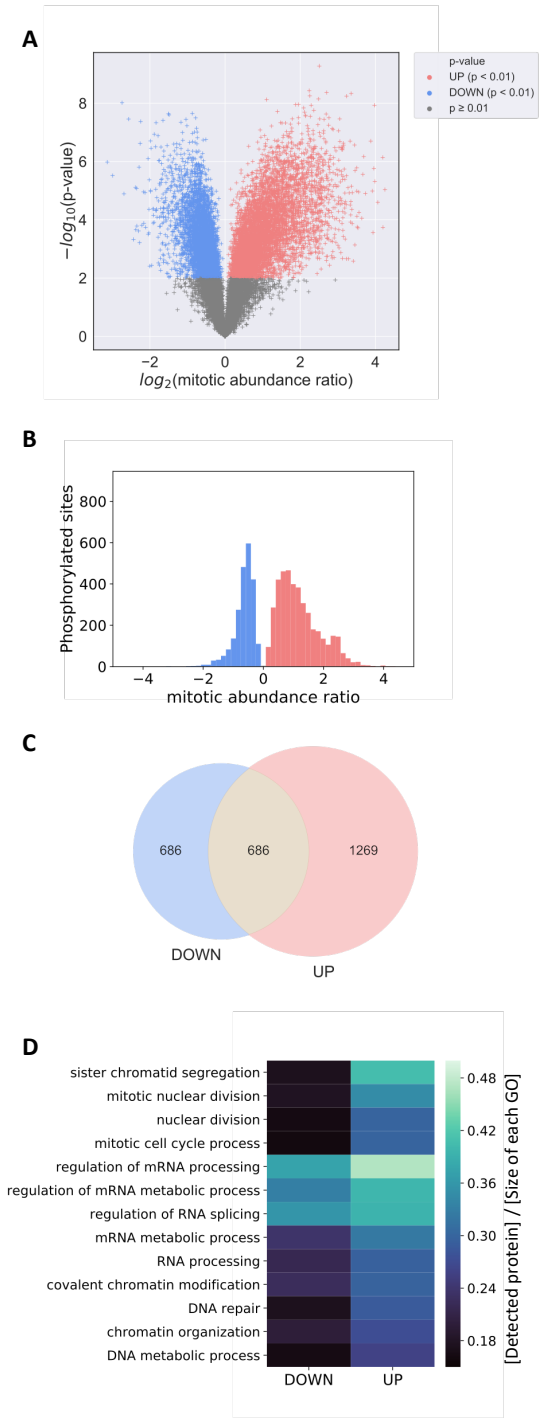

Yamazaki et al. Figure 1

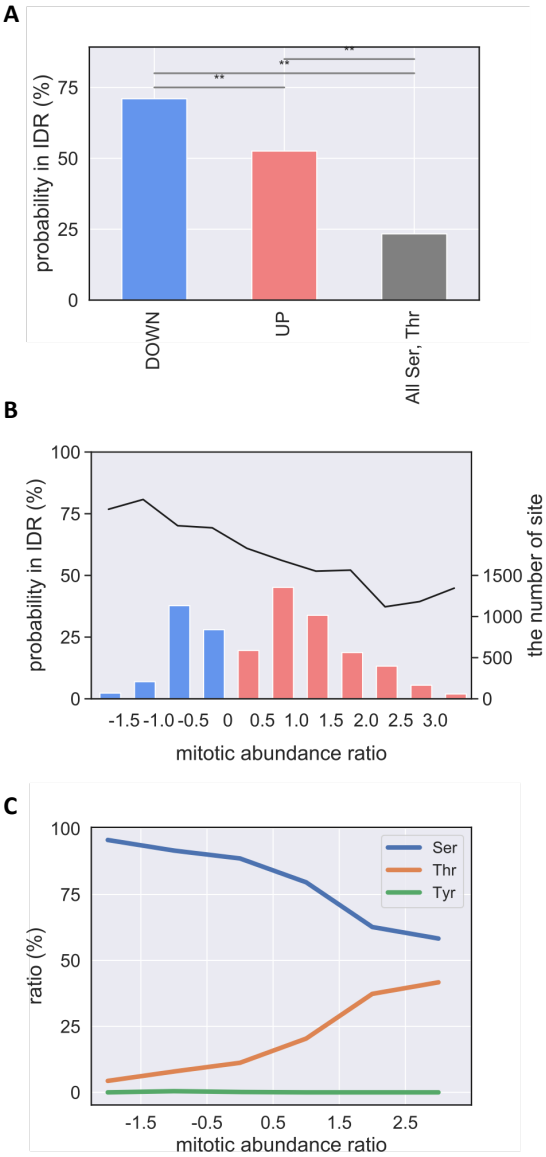

Yamazaki et al. Figure 2

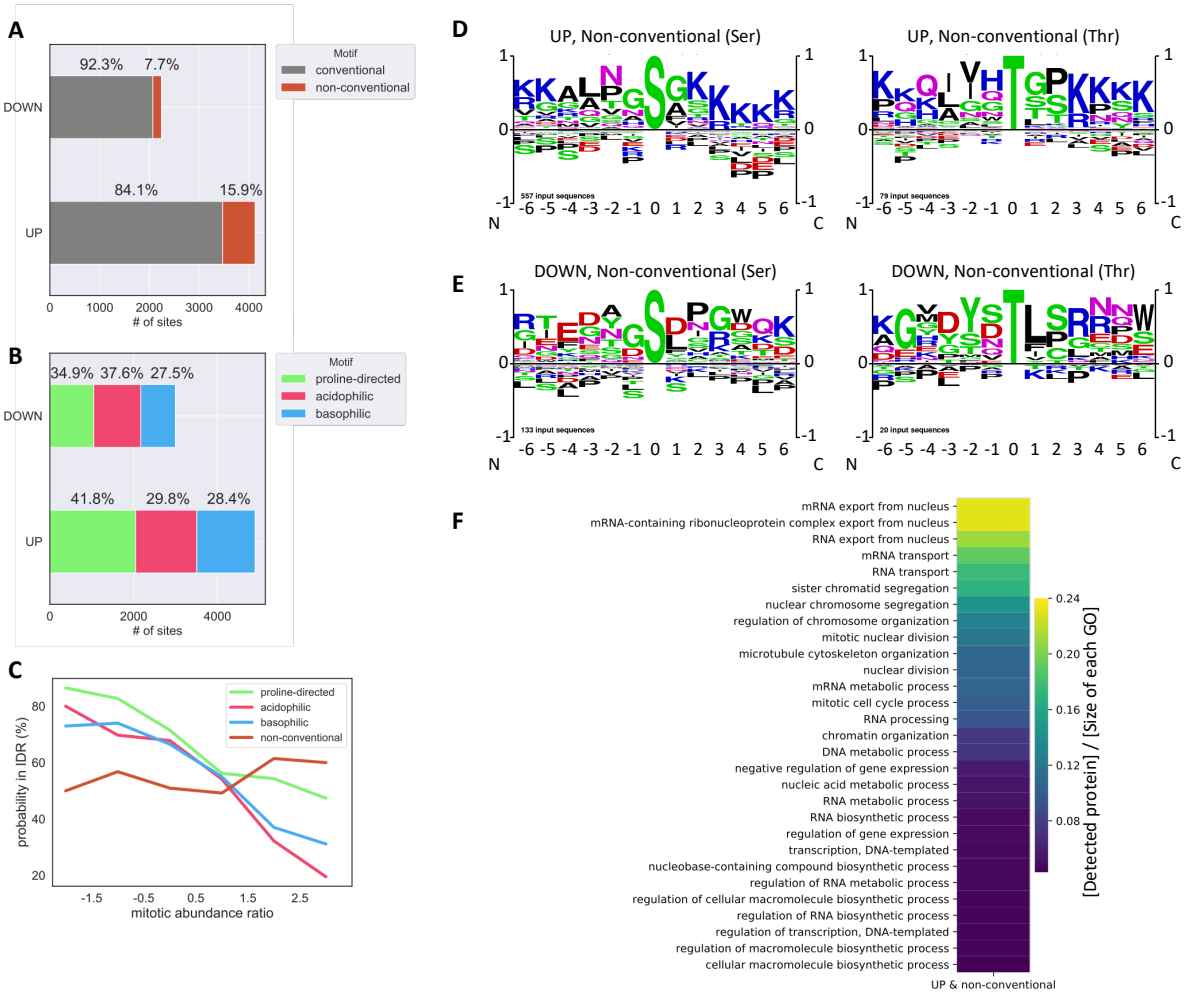

Yamazaki et al. Figure 3

517 # Figure and Figure Legends

518

519 **Figure 1. Quantification of mitotic phosphorylation by tandem mass tag analysis**

520 (A) A volcano plot of TMT-analysis. The p-value and the abundance ratio of individual phosphopeptides were
521 plotted. The peptides with the p-value lower than 2 (grey) were eliminated from the subsequent analyses. The
522 peptides with positive (red) and negative (blue) were extracted and were subjected to the subsequent analyses.
523 (B) Histogram of the abundance ratio. UP (red) and DOWN (Blue) sites are distinguished.
524 (C) Venn diagram of the number of proteins carrying UP and/or DOWN sites.
525 (D) Gene ontology analysis of phosphoproteins carrying UP or DOWN sites. Biological process term were
526 obtained from DAVID. The number of proteins identified in this study was divided by the number of total
527 proteins in each term. Shown here are several terms relatively abundant UP and DOWN sites.

528

529 **Figure 2. Structural properties of mitotic phosphosites.**

530 (A) The probability of phosphosites existing in intrinsically disordered regions. The IDR probabilities of all
531 serine and threonine residues, all phosphosites, UP sites and DOWN sites are plotted.
532 (B) The relationship between IDR probability and the abundance ratio.
533 (C) The relationship between the amino acid residue of phosphosites and the abundance ratio.

534

535 **Figure 3. Neighboring sequences of mitotic phosphosites**

536 (A, B) The ratio of conventional and non-conventional motifs (A) and the ratio of individual conventional
537 motifs (B) in UP and DOWN sites.
538 (C) The relationship between the IDR probability and the abundance ratio was analyzed for individual
539 conventional motifs and non-conventional motif.
540 (D, E) Logo analysis of flanking residues of UP (D) and DOWN (E) sites in non-conventional motif. The
541 results for phosphoserine (left) and phosphothreonine (right) are shown.
542 (F) Gene ontology (biological process) analysis on proteins with UP sites in non-conventional motif. The
543 number of proteins identified was divided by the total number of proteins in each term.

544

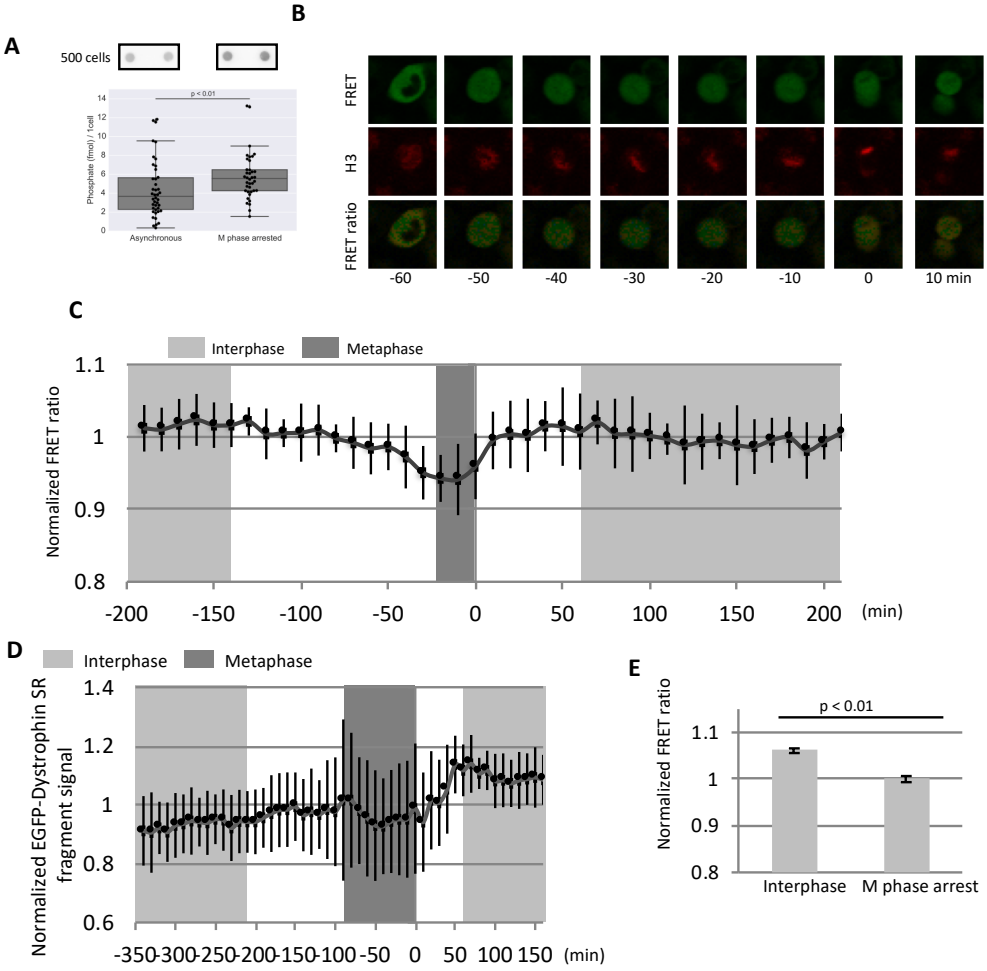

Yamazaki et al. Figure S1

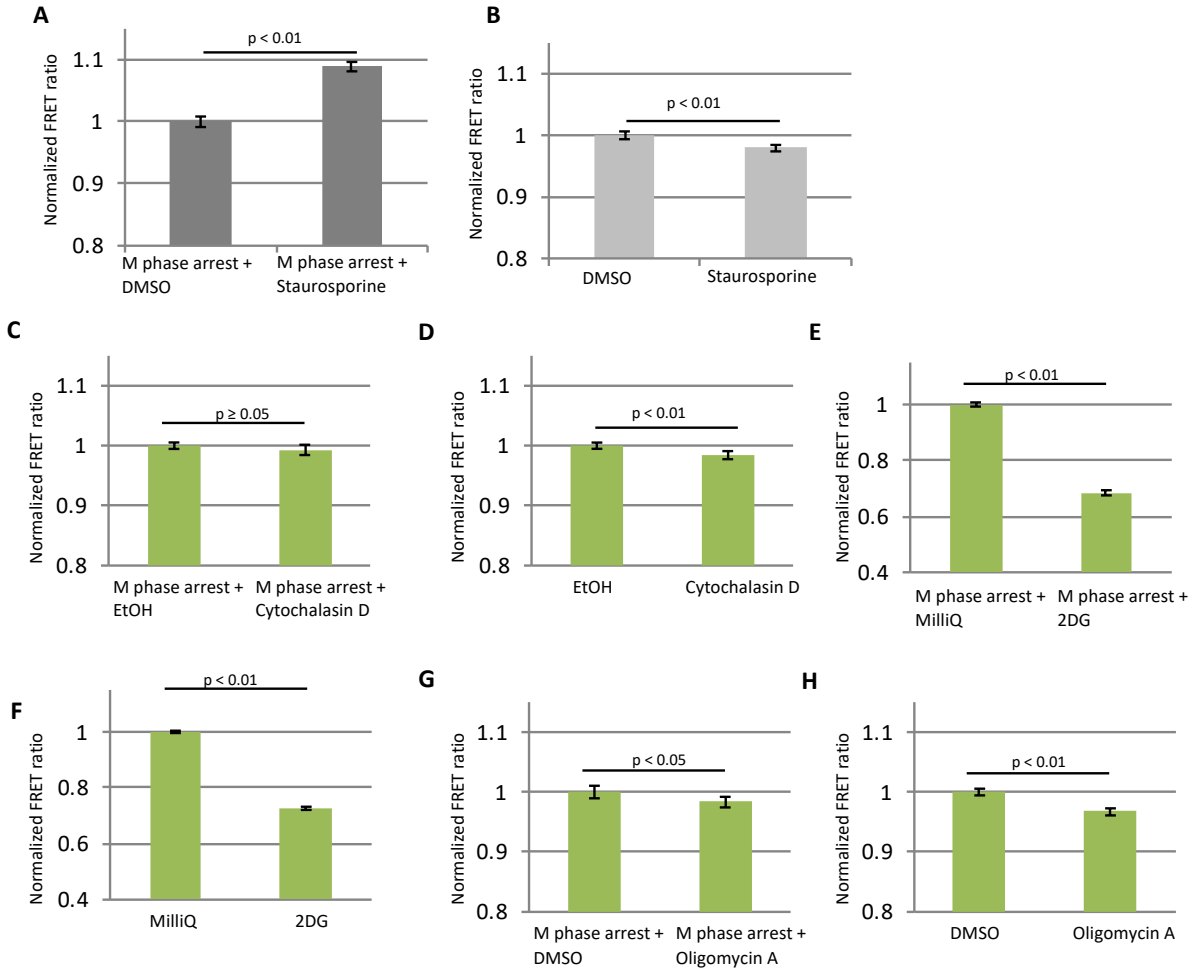

Yamazaki et al. Figure S2

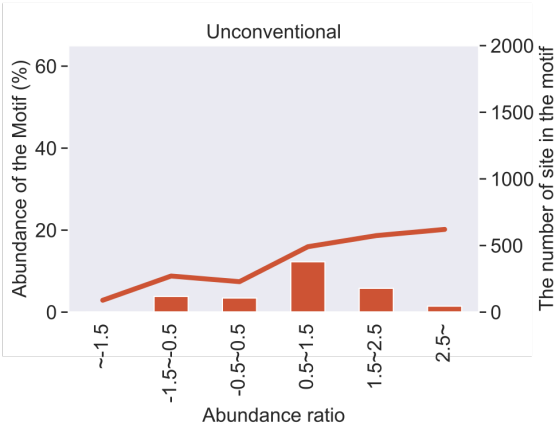

Yamazaki et al. Figure S3

548 # Supplemental Figure, Table and Legends

549 **Figure S1. Total amount of phosphoprotein increases and intracellular ATP level decreases during**
550 **mitosis.**

551 (A) The amount of phosphate on proteins in asynchronous and nocodazole-treated HeLa cells was quantified
552 using pIMAGO and streptavidin HRP conjugate. Dot-blot analysis of the cell lysate from 500 cells is shown
553 here. The data points are obtained from three independent experiments and outlier was eliminated at each
554 experiment using method of a function of the inter-quartile range. The significance was tested by Mann–
555 Whitney U-test.

556 (B, C) Quantification of the cytoplasmic ATP level during mitosis. HeLa cells expressing ATeam and mPlum-
557 Histone H3 were observed by live-cell time-lapse imaging. Representative fluorescence images of FRET
558 signal, mPlum signal and acceptor/donner ratio are shown (B). Time 0 is defined when chromosomes started
559 to segregate at anaphase onset. The acceptor/donner ratio was quantified in images, normalized to that in
560 interphase, and plotted against time (C). Data was collected from 16 cells and each data points has at least 8
561 cells. Error bars represents S.D.

562 (D) The experiment described in Fig S1B was performed with EGFP-tagged dystrophin. Data was collected
563 from 13 cells and each data points has at least 7 cells. Error bars represent S.D.

564 (E) Comparison of cytoplasmic ATP level between non-treated and nocodazole-treated HeLa cells. HeLa cells
565 expressing ATeam were treated with 2 mM thymidine for 18 hours and released to DMEM with 10% FBS for
566 1 hour. Then cells were treated with or without 0.2 μM nocodazole for 10 hours, and observed by confocal
567 fluorescence microscopy. The acceptor/donner ratio was quantified in the obtained images and summarized.
568 Data was collected from more than 100 cells. The value was normalized by that of nocodazole-treated cells.
569 The reduction of signal in mitosis was observed as is the case in living cells shown in B and C. Error bars
570 represent 95% CI. The significance was tested by Welch's t-test.

571

572 **Figure S2. Protein phosphorylation decreases the intracellular ATP level during mitosis.**

573 The experiment described in Fig. S1D was performed in the presence of various inhibitors in M-phase
574 arrested cells (A, C, E, G) and non-synchronized cells (B, D, F, H). For M-phase arrest, HeLa cells were
575 treated with thymidine for 18 hours, and, after incubation with normal medium for 1 hour, treated with 0.2
576 μM nocodazole for 10 hours.

577 (A, B) Cells were treated with 1 μM Staurosporine, an inhibitor of for 1 hour.

578 (C, D) Cell were treated with 1 μM Cytochalasin D, an inhibitor of actin polymerization, for 1 hour.

579 (E, F) Cells were treated with 10 mM 2-deoxy-D-glucose (2DG), an inhibitor of glycolysis for 1 hour.

580 (G, H) Cells were treated with12.6 μM Oligomycin A, an inhibitor of oxidative phosphorylation, for 1 hour.
581 The acceptor/donner ratio was quantified in the obtained images, and normalized by that in the absence of the
582 inhibitor. Error bars represent 95% CI. The significance was tested with Welch's t-test.

583

584 **Figure S3. Occupancy of non-conventional motif against early mitotic abundance ratio**

585 The occupancy of sites in non-conventional motif was increase along with early mitotic abundance ratio

586

587 **Table S1. Proteins with UP non-conventional motif, which are phosphorylated by AMPK.**

588 42 proteins with UP non-conventional motif have been identified as the substrates of AMPK in previous

589 report.